

**AFRL-AFOSR-UK-TR-2011-0033**



## **Re-addressable Interconnects with Light-Induced Waveguides in Liquid Crystals**

**Gaetano Assanto**

**University Roma Tre  
Department of Electronic Engineering  
Via della Vasca Navale 84  
Rome, Italy 00146**

EOARD GRANT 10-3010

August 2011

Final Report from 01 September 2010 to 31 August 2011

**Distribution Statement A: Approved for public release distribution is unlimited.**

**Air Force Research Laboratory  
Air Force Office of Scientific Research  
European Office of Aerospace Research and Development  
Unit 4515 Box 14, APO AE 09421**

**REPORT DOCUMENTATION PAGE**

Form Approved OMB No. 0704-0188

Public reporting burden for this collection of information is estimated to average 1 hour per response, including the time for reviewing instructions, searching existing data sources, gathering and maintaining the data needed, and completing and reviewing the collection of information. Send comments regarding this burden estimate or any other aspect of this collection of information, including suggestions for reducing the burden, to Department of Defense, Washington Headquarters Services, Directorate for Information Operations and Reports (0704-0188), 1215 Jefferson Davis Highway, Suite 1204, Arlington, VA 22202-4302. Respondents should be aware that notwithstanding any other provision of law, no person shall be subject to any penalty for failing to comply with a collection of information if it does not display a currently valid OMB control number.

**PLEASE DO NOT RETURN YOUR FORM TO THE ABOVE ADDRESS.**

<b>1. REPORT DATE (DD-MM-YYYY)</b> 09-08-2011	<b>2. REPORT TYPE</b> Final Report	<b>3. DATES COVERED (From – To)</b> 1 September 2010 – 31 August 2011
--	---------------------------------------	--

<b>4. TITLE AND SUBTITLE</b>  <b>Re-addressable Interconnects with Light-Induced Waveguides in Liquid Crystals</b>	<b>5a. CONTRACT NUMBER</b> FA8655-10-1-3010
	<b>5b. GRANT NUMBER</b> <b>Grant 10-3010</b>
	<b>5c. PROGRAM ELEMENT NUMBER</b>

<b>6. AUTHOR(S)</b>  Professor Gaetano Assanto	<b>5d. PROJECT NUMBER</b>
	<b>5d. TASK NUMBER</b>
	<b>5e. WORK UNIT NUMBER</b>

<b>7. PERFORMING ORGANIZATION NAME(S) AND ADDRESS(ES)</b> University Roma Tre Department of Electronic Engineering Via della Vasca Navale 84 Rome, Italy 00146	<b>8. PERFORMING ORGANIZATION REPORT NUMBER</b>  N/A
--	--

<b>9. SPONSORING/MONITORING AGENCY NAME(S) AND ADDRESS(ES)</b>  EOARD Unit 4515 BOX 14 APO AE 09421	<b>10. SPONSOR/MONITOR'S ACRONYM(S)</b> AFRL/AFOSR/RSW (EOARD)
	<b>11. SPONSOR/MONITOR'S REPORT NUMBER(S)</b> <b>AFRL-AFOSR-UK-TR-2011-0033</b>

**12. DISTRIBUTION/AVAILABILITY STATEMENT**  
Approved for public release; distribution is unlimited. (approval given by local Public Affairs Office)

**13. SUPPLEMENTARY NOTES**

**14. ABSTRACT**  
The theoretical and numerical analyses carried out with reference to finite light beams in anisotropic dielectrics enable us to deal with narrow beams in the non-paraxial approximation, both in the linear and in the nonlinear regimes, detailing roles and contributions of the uniaxial response, the induced non-locality, the asymmetry introduced by non-negligible longitudinal field components and the second derivatives in propagation. The detailed analysis of reorientational nematic liquid crystals allows us to model self-steering of spatial solitons in media with power-dependent walk-off via reorientation of the optic, a regime effectively addressable in experimental samples with E7 and planar geometries.  
In the second phase investigated soliton self-steering in undoped nematic liquid crystals with various initial orientations in the plane of propagation, i.e. self-deflection of nematicons owing to power-dependent reorientation of the optic axis. Introduced perturbative and nonperturbative regimes, the latter accounting for all-optical changes in walk-off. Reduced the complete 3D system to an equivalent 2D model retaining nonlocality. In the perturbative regime, found two scalar parameters describing soliton waist and walk-off versus  $\theta_0$ . To verify the predictions, experimentally investigated nematicon propagation and self-steering in samples with various  $\theta_0$ , obtaining an excellent agreement between data and analysis even in the presence of scattering losses which induce a decay of the nonlinear response along propagation. In the last phase introduced a novel concept for optical signal steering using spatial solitons and a voltage-tunable interface in nematic liquid crystals. The design ensures in-plane self-confined and signal guiding propagation and deflection over angles as large as  $70^\circ$  by employing modest voltages, enabling the realization of re-addressable interconnections and spatial demultiplexers with a wide angular span while guaranteeing the transparent transmission of one or several signals with arbitrary wavelengths and modulations.

**15. SUBJECT TERMS**  
EOARD, Liquid Crystals, Laser beam control

<b>16. SECURITY CLASSIFICATION OF:</b>			<b>17. LIMITATION OF ABSTRACT</b>  SAR	<b>18. NUMBER OF PAGES</b>  28	<b>19a. NAME OF RESPONSIBLE PERSON</b> A. GAVRIELIDES
<b>a. REPORT</b> UNCLAS	<b>b. ABSTRACT</b> UNCLAS	<b>c. THIS PAGE</b> UNCLAS			<b>19b. TELEPHONE NUMBER</b> (Include area code) +44 (0)1895 616205

**Grant # FA8655-10-1-3010**

**NATO-EOARD Project**

**“Re-addressable Interconnects with Light-induced Waveguides in Liquid Crystals”**

## **First Periodic Report**

**Prof. Gaetano Assanto**

**Nonlinear Optics and OptoElectronics Lab**

Department of Electronic Engineering, University Roma Tre  
Via della Vasca Navale 84, 00146 Rome- ITALY

### **Table of Contents**

- Summary
- 1. Introduction
- 2. Methods, Assumptions, and Procedures
  - Self-Localized light propagation
- 3. Results and Discussion
  - 3.1 Non paraxial beam propagation in uniaxial media
  - 3.2 Spatial optical solitons in nematic liquid crystals
- 4. Conclusions
- 5. References
- 6. List of Figures
- List of Symbols, Abbreviations and Acronyms
- Appendix: confirmation of expenditures

### **Summary**

In the first four months of the Project, various aspects of light self-localization in reorientational Kerr-like media such as nematic liquid crystals have been examined, including issues related to the propagation of narrow beams besides the paraxial approximation as well as self-acceleration of self-confined light beams in Kerr anisotropic dielectrics.

The samples were provided through collaborations the University of Southampton (UK), the Institut Non Lineaire de Nice (Sophia Antipolis, France)) and BEAM-Engineering (Orlando, USA). After a brief introduction, we recall the basic concepts on self-localized propagation of light beams in media with a reorientational response; then we illustrate numerical and theoretical analyses and some experimental results on self-steered self-confined light beams, i.e. self-accelerating spatial solitons, in nematic liquid crystals (LC).

### **1 Introduction**

Coupling and routing light for optical telecommunications and on-chip signal processing is currently mostly based on static couplers or opto-electric and electro-optical converters. Experiments in LC have proven that two-dimensional solitons are "robust" entities, can survive index non-homogeneities (lens-like, interfaces or other solitons), can confine weaker signals with a smooth transverse profile, can be steered and routed in space by externally controlled parameters, including temperature, voltage, extra beams.<sup>1-3</sup> Owing to self-healing upon propagation,<sup>4</sup> liquid crystals soliton-induced waveguides can tolerate alignment and angular offsets, as well as polarization noise. While optical spatial solitons reported so far in

liquid crystals have been shown to react to external stimuli, their performance is far from optimal: their response time can be larger than 100ms and they exhibit transverse fluctuations due to non-locality and the liquid phase of the supporting medium. Overcoming the current limits is necessary to realize competitive and all-optical signal interconnects. Based on recent progress spatial optical solitons in nematic liquid crystals, spatially stable waveguides induced by self-trapped light beams can be envisioned as a novel photonic platform for dynamically re-addressable broadband optical signal interconnects.

As anisotropic molecular systems are amenable to the definition and tuning of arbitrary refractive index distributions by external voltages and light-induced reorientation, in this Project we aim at verifying models for the exploitation of electro-optic, as well as opto-optic, control of soliton waveguides and circuits in nematic liquid crystals, including light-valves with photosensitive layers.<sup>5</sup> The merging of non-local/electro-optic/non-linear material properties and engineered/tunable refractive index distributions is meant to naturally eliminate some drawbacks of free-space propagation and offer more versatility than built-in integrated optical interconnects. Moreover, the intrinsic self-collimation (guidance) characteristic of bright solitons will reduce signal attenuation, ensure a smooth transverse profile ideal for in-fibre coupling, reduce polarization noise and allow large deflections in engineered structures.

Such new photonic platform and interconnect approach requires an in-depth analysis of the intricate interplay between non-linear light propagation in non-local media, the interaction of light with boundaries, refractive index profiles, external voltages and other light beams.

## 2 Methods, Assumptions, and Procedures

The Project aims at demonstrating the feasibility of optical and all-optical signal processing for network reconfiguration in compact microsystems based on light self-localization and power-controlled self-steering using liquid crystal technology and liquid crystalline materials, specifically nematic liquid crystals.

The two main routes of investigation undertaken during the first four months were:

**- 1: Light propagation and localization in non-local molecular media:** we focus on theory, simulation, design, realization and characterization of individual waveguides based on spatial optical solitons in nematic liquid crystals, i.e. Nematicons.<sup>6</sup> Beam propagation models and software will be used to analyze and design the required refractive index distributions, modelling the effects of non-locality and the role of tight (self-) confinement. We will identify and prepare the samples to be assembled in two main geometries - namely planar cells and planar photoconductive light valves - for optoelectronic characterization. The basic elements will be characterized in terms of excitation, profile, spatial response etc.

**- 2: Steering and routing with optical spatial solitons:** we focus on theory, simulation, design, realization and characterization of different ways for transverse self-acceleration of Nematicons, obtained to date by:

- mutual interaction of solitons in nonlocal dielectrics<sup>7-10</sup>
- voltage control<sup>11-14</sup>;
- light control<sup>15-18</sup>.

## 3. Results and Discussion

### 3.1 Non paraxial beam propagation

Since the excitation and propagation of optical spatial solitons in nematic liquid crystals involves beam self-confinement via a reorientational nonlinearity with a strong nonlocal

character, nematicons are expected to breath in waist as they propagate and self-focus to transverse size comparable or even narrower than the wavelength of light. The latter feature demands a detailed investigation of narrow beam propagation, as their reduced waist fails to comply with the usually adopted scalar or paraxial approximation and the slowly varying envelope approximation.<sup>20-21</sup>

In the study of paraxial beams in isotropic homogeneous media, scalar Hermite-Gaussian beams are essential, as they form a complete set: when dealing with one-directional (1+1)D propagation, every initial profile can be expressed as a superposition of HG eigen-beams. Focusing on a (1+1)D geometry, we demonstrate that the fully vectorial problem of light beam evolution in uniaxials, when excited by extraordinary waves undergoing a finite walk-off, can be exactly reduced to a single scalar Helmholtz equation for the magnetic field, even in the non-paraxial limit.

We consider a homogeneous non-magnetic crystalline dielectric encompassing a single optic axis and in the presence of a harmonic electromagnetic perturbation, with constitutive relations  $\mathbf{B} = \mu\mathbf{H}$  and  $\mathbf{D} = \epsilon_0\epsilon \cdot \mathbf{E}$ . We name  $\epsilon_{\perp}$  and  $\epsilon_{\parallel}$  the eigenvalues of  $\epsilon$  with multiplicity two and one, respectively, and define the birefringence  $\epsilon_a = \epsilon_{\parallel} - \epsilon_{\perp}$ . For simplicity, we take the optic axis lying in the plane  $yz$  and a (1+1)D geometr, such that two independent solutions exist for Maxwell's equations: ordinary (-o)) and extraordinary (-e) waves, respectively. Light propagation is governed by two Helmholtz's equations. In a rotated reference system introduced to handle e-waves, o-solutions can be found by duality, i.e. exchanging  $\mathbf{E}$  with  $\mathbf{H}$  and viceversa from the e-case and  $\epsilon_{yz}=0$  (no walkoff).

Adopting a reference system  $xts$ , with  $s$  along the Poynting vector  $\mathbf{S}$  and  $t$  orthogonal to it, the electric field components take a relatively simple form and the flux of  $\mathbf{S}$  through a close volume is purely reactive, in agreement with energy conservation in the stationary regime. For a finite beam and an arbitrary direction  $z$ , we can address the effects of anisotropy on the symmetry of the Poynting vector. We consider an input magnetic field  $\mathbf{A}$  of given parity: such solution of a Helmholtz's equation will retain its symmetry while propagating. For a light beam with mean wavevector along  $z$  and its corresponding Poynting vector along  $s$ , a symmetry breaking takes place in anisotropic dielectrics where the walkoff is nonzero and its effects increase with the beam divergenc, i.e. its spatial spectrum.

Considering a narrow beam with an initial profile given by a HG function, we use a numerical expansion of the angular spectrum to solve the propagation problem exactly, focusing on the lowest-order Gaussian input profile with initial waist  $w_0$  and a flat phase profile.

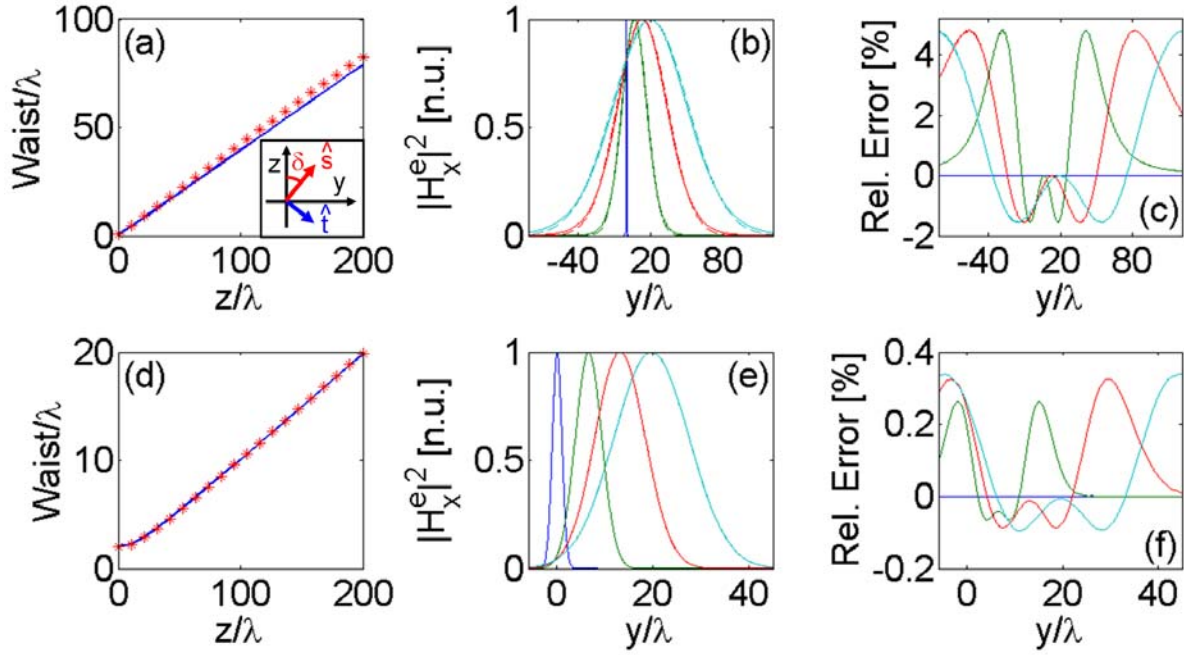


Fig. 1 (a, d) Beam waist vs  $z$ ; blue solid lines and red symbols refer to paraxial Gaussian beams and numerical solutions, respectively. (b, e)  $H_x^e$  vs  $y/\lambda$ , normalized to its peak and computed for (from left to right)  $z/\lambda = 0, 53, 105, 158$ ; solid and dashed lines are HG profile and numerical solutions, respectively. (c, f) Relative error between the profiles in (b, e). Top and bottom graphs are computed for  $w_0/\lambda = 0.5$  and  $w_0/\lambda = 2$ , respectively. Here  $\varepsilon_{||} = 2.89$ ,  $\varepsilon_{\perp} = 2.25$ . Inset: unit vectors  $s$  and  $t$ .

The numerical solutions confirm the theoretical predictions: the magnetic field walks-off and retains its even symmetry even in the highly non-paraxial limit. As visible in Fig.1, going from large waists down, the effects of the second partial derivative of  $A$  along the propagation  $z$  are negligible up to the wavelength  $\lambda$ ; for  $w/\lambda = 2$  the relative error is  $< 1\%$ , whereas for  $w/\lambda = 0.5$  the differences between the two models remain small, with a relative error on waist  $< 8\%$  (Fig.1). The trend is confirmed by Fig.1(c-f) plotting the relative error between paraxial and non-paraxial  $H_x$ . The agreement between numerical simulations and HG profile for large  $w/\lambda$  confirms that the slowly-varying-envelope approximation needs be applied along in the moving reference system. Fig. 2(a) plots  $\text{Re}(\mathbf{S})$  along  $s$ , corresponding to  $H_x$  in Fig. 1(a): the energy propagates at the walk-off angle. Both the ratios between the longitudinal  $E_s$  and the transverse  $E_t$  electric field components and between odd and even parts of  $\text{Re}(\mathbf{S})$  are inversely proportional to  $w_0$  [Fig.2 (c, d)], with the former one order of magnitude larger than the latter.

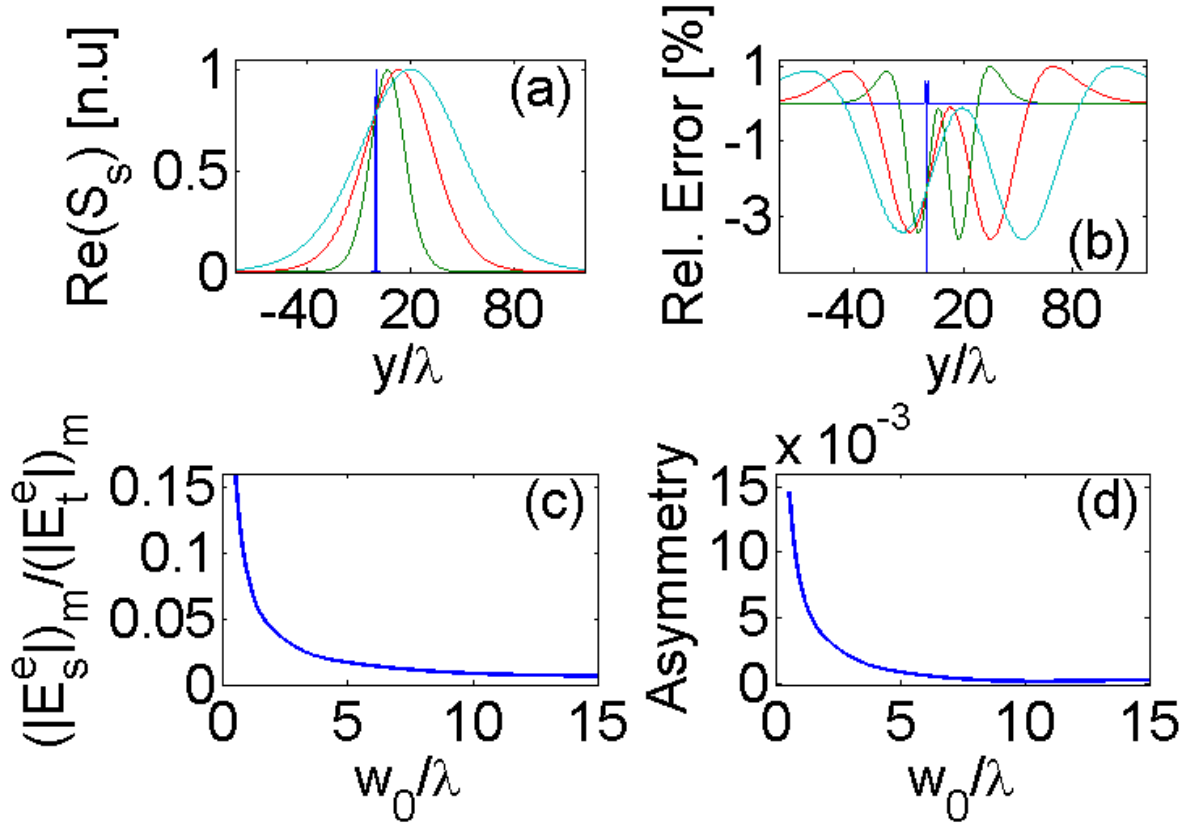


Fig. 2 (a) Computed transverse profile of  $\text{Re}(\mathbf{S})$  along  $s$  and (b) relative error with respect to the paraxial expression for  $w/\lambda=0.5$ ;  $\text{Re}(\mathbf{S})$  is normalized to its peak for fixed  $z$  and each curve corresponds to the same  $z/\lambda$  of Fig. 1. (c) Ratio of maxima of  $|E_t|$  and  $|E_s|$  for fixed  $z$  and (d) ratio between maxima of odd and even parts of  $\text{Re}(\mathbf{S})$  vs  $w_0/\lambda$ .

A direct comparison of Fig. 1 (c, f) with Fig. 2 (c) reveals that the differences between scalar (paraxial) and full vectorial model solutions are larger than the corrections due to the second longitudinal derivative, in agreement with Ref. 20.

### 3.2 Spatial optical solitons in nematic liquid crystals

In many cases the nonlinear effects are related to the anisotropy of the material, such as in reorientational media and nematic liquid crystals.<sup>3,8,12,19</sup> Spatial solitons in the paraxial regime are often modelled by a scalar NL Schroedinger equation.

We extended the analysis summarized in the previous section and investigated bright single-hump symmetrically-shaped spatial solitons in uniaxial media by solving Maxwell's equations in geometries where ordinary and extraordinary polarization components are decoupled, studying non-perturbative regimes where linear and NL polarizations become comparable in magnitude and showing how non-paraxiality results in an effective nonlocality even in local media.

In particular, in the highly NL regime relevant to nematic liquid crystals (NLC) -among other NL dielectrics-, we expect soliton self-steering via power-controlled changes in walk-off.

NLC are known to exhibit very high effective nonlinearities (typically  $10^6 \text{ cm}^2/\text{W}$ ) due to the particular nature of light-matter interactions.<sup>22</sup> As a consequence, in uniaxial NLC the optic axis (or molecular director) can reorientate in space by reacting to the electric fields of light beams in the milliwatt or even microwatt range<sup>17</sup>: when the induced rotation becomes comparable with the initial distribution, the nonlinear polarization is no longer negligible with respect to the linear one. Light self-steering owing to nonlinear changes in walk-off was experimentally demonstrated in the modulational instability regime.<sup>23, 24</sup> NLC behave as a

saturable nonlocal nonlinear medium able to support stable (2+1)D spatial solitons at relatively low cw excitations. At low powers, the soliton trajectories do not bend because of the negligible walk-off variations associated with the optically-induced reorientation,<sup>11</sup> at higher powers, beam self-bending can be expected.

We refer to a planar NLC cell, infinitely extended along  $y$  and  $z$  and with a finite thickness  $L$  across  $x$ .<sup>8</sup> The boundary conditions induce a homogeneous director distribution in the absence of excitation, with the optic axis lying in the plane  $yz$  at an angle  $\theta_0$  with respect to  $z$ . Maxwell's equations need be solved in conjunction with those ruling the director distribution; since the electric field vector belongs to the plane  $yz$ , the director remains coplanar at an angle  $\theta$  with respect to the axis  $z$ . The angle  $\theta$  is governed by

$$K\nabla^2\theta + \epsilon_a [\sin(2\theta) (|E_y|^2 - |E_z|^2) + 2\text{Re}(E_y E_z^*) \cos(2\theta)] = 0$$

with  $K$  the Frank elastic constant (for molecular deformations). We look for single-hump solitary solutions having a flat-phase transverse profile, indicating with  $\delta=\delta(\theta)$  the (power dependent) walk-off. Therefore, we fix the wavevector and allow the Poynting vector to change its direction in  $yz$ , consistently with typical experimental set-ups.<sup>8,11</sup> Due to the high-nonlocality of this medium,<sup>19</sup> to compute the soliton profile we can take for  $\delta$  and the extraordinary refractive index the value computed at the beam peak (solitons are even owing to symmetry). In other words, assuming known the distribution of  $\theta$  in the self-localization regime, we can consider the latter an inhomogeneous distribution of the optic axis, and keep into account that the nonlinear perturbations are perceived as small by the soliton because of the high nonlocality; hence, only transverse variations in the refractive index are relevant.

In order to get a simplified (1+1)D model for nonlinear optical propagation, for the  $x$ -dependence of the optical perturbation we make the ansatz  $\sin(\pi x/L)$  (the cell boundaries are in  $x=0,L$ ) and consider beams propagating in the cell mid-plane  $x=L/2$ .

Fig. 3 shows numerical solutions for  $\theta_0=\pi/4$ : due to the reorientational nonlinearity, the induced optical perturbation saturates at high power, resulting in a non-monotonic trend for the soliton waist with power [see Fig. 3(a)].

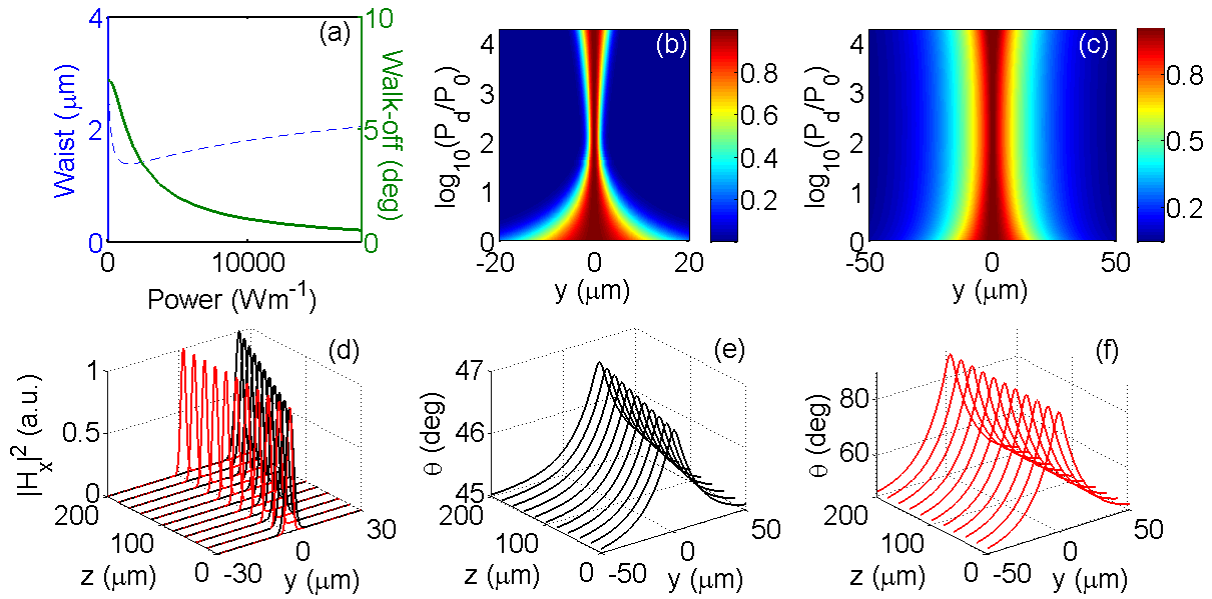


Fig. 3 Soliton self-steering in NLC. (a) Soliton waist (dashed blue line) and walk-off (solid green line) versus power density. (b) Plots of  $|H_x|$  and the optical perturbation  $\Delta\theta$  in the soliton case, versus  $y$  and the logarithm of the power density  $P_d$ , with  $P_d=62$  W/m. Both quantities are normalized to their peak value at each power. (d) Beam evolution in  $yz$  computed by BPM when the input profile corresponds to a solitary solution for  $P_d=62$  W/m (black lines, beam with the largest slope in  $yz$ ) and  $P_d=1.8 \cdot 10^4$  W/m (red lines). (c) and (d) show the corresponding perturbation in the director distribution in the cell.

Fig. 3(a) graphs also the walk-off  $\delta$  versus power, demonstrating soliton self-bending. Fig. 5 (c-d) plot the profiles of the field and  $\Delta\theta$  versus the transverse coordinate  $y'$  and power density  $P_d$ : the field profile is very close to Gaussian due to the high nonlocality of NLC, whereas the optical perturbation  $\Delta\theta$  is very similar to the Green function of the structure with a width slightly changing versus power, exponentially decreasing for large  $|y'|$  with a slope determined by  $L$ . Using a BPM propagator with a relaxation algorithm to calculate the director distribution in  $yz$ , we checked that the calculated solutions effectively correspond to solitons by simulating their propagation in an NLC cell. As shown in Fig. 5 (d), the beams walk-off with invariant profiles, confirming the validity of the computed solutions and the occurrence of power-dependent angular self-steering.

## 4 Conclusions

The theoretical and numerical analyses carried out with reference to finite light beams in anisotropic dielectrics enable us to deal with narrow beams in the non-paraxial approximation, both in the linear and in the nonlinear regimes, detailing roles and contributions of the uniaxial response, the induced nonlocality, the asymmetry introduced by non-negligible longitudinal field components and the second derivatives in propagation. The detailed analysis of reorientational nematic liquid crystals allows us to model self-steering of spatial solitons in media with power-dependent walk-off via reorientation of the optic, a regime effectively addressable in experimental samples with E7 and planar geometries.

## 5. References

- <sup>1</sup> Yu. S. Kivshar and G. P. Agrawal, *Optical Solitons: From Fibers to Photonic Crystals* (Academic, San Diego, 2003)
- <sup>2</sup> G. I. Stegeman and M. Segev, *Science* **286**, 1518 (1999)

- <sup>3</sup> C. Conti and G. Assanto, in *Encyclopedia of Modern Optics*, Vol. 5, pp. 43-55, edited by R. D. Guenther, D. G. Steel and L. Bayvel, (Elsevier, Oxford, 2004)
- <sup>4</sup> A. Alberucci, M. Peccianti, G. Assanto, G. Coschignano, A. De Luca and C. Umeton, *Opt. Lett.* **30**, 1381 (2005)
- <sup>5</sup> A. Piccardi, U. Bortolozzo, S. Residori and G. Assanto, *Opt. Lett.* **34**, 737 (2009)
- <sup>6</sup> G. Assanto and M. Karpierz, *Liq. Cryst.* **36**, 1161 (2009)
- <sup>7</sup> M. Peccianti, K. A. Brzdąkiewicz, and G. Assanto, *Opt. Lett.* **27**, 1460 (2002)
- <sup>8</sup> M. Peccianti, C. Conti, G. Assanto, A. De Luca and C. Umeton, *Appl. Phys. Lett.* **81**, 3335 (2002)
- <sup>9</sup> A. Fratolocchi, A. Piccardi, M. Peccianti and G. Assanto, *Opt. Lett.* **32**, 1447 (2007)
- <sup>10</sup> Y. Izdebskaya, V. Shvedov, A. S. Desyatnikov, Y. S. Kivshar, W. Krolikowski, and G. Assanto, *J. Eur. Opt. Soc.* **5**, 10008 (2008)
- <sup>11</sup> M. Peccianti, C. Conti, G. Assanto, A. De Luca and C. Umeton, *Nature (London)* **432**, 733 (2004)
- <sup>12</sup> G. Assanto, C. Umeton, M. Peccianti and A. Alberucci, *J. Nonl. Opt. Phys. Mat.* **15**, 33 (2006)
- <sup>13</sup> M. Peccianti, A. Dyadyusha, M. Kaczmarek and G. Assanto, *Nat. Phys. (London)* **2**, 737 (2006)
- <sup>14</sup> M. Peccianti, A. Dyadyusha, M. Kaczmarek, and G. Assanto, *Phys. Rev. Lett.* **101**, 153902 (2008)
- <sup>15</sup> M. Peccianti and G. Assanto, *Opt. Lett.* **30**, 2290 (2005)
- <sup>16</sup> A. Pasquazi, A. Alberucci, M. Peccianti and G. Assanto, *Appl. Phys. Lett.* **87**, 261104 (2005)
- <sup>17</sup> S. V. Serak, N. V. Tabiryan, M. Peccianti and G. Assanto, *IEEE Photon. Techn. Lett.* **18**, 1287 (2006)
- <sup>18</sup> A. Piccardi, G. Assanto, L. Lucchetti and F. Simoni, *Appl. Phys. Lett.* **93**, 171104 (2008)
- <sup>19</sup> C. Conti, M. Peccianti and G. Assanto, *Phys. Rev. Lett.* **91**, 073901 (2003)
- <sup>20</sup> M. Lax, W. Louisell and W. McKnight, *Phys. Rev. A* **11**, 1365 (1975)
- <sup>21</sup> G. Agrawal and D. Pattanayak, *J. Opt. Soc. Am.* **69**, 575 (1979)
- <sup>22</sup> N. V. Tabiryan, *Mol. Cryst. Liq. Cryst.* **62**, 237 (1980)
- <sup>23</sup> M. Peccianti, C. Conti and G. Assanto, *Phys. Rev. E* **68**, 025602(R) (2003)
- <sup>24</sup> M. Peccianti and G. Assanto, *Opt. Lett.* **30**, 2290 (2005)

## 6. List of figures

Fig. 1 (a, d) Beam waist vs  $z$ ; blue solid lines and red symbols refer to paraxial Gaussian beams and numerical solutions, respectively. (b, e)  $H_x^2$  vs  $y/\lambda$ , normalized to its peak and computed for (from left to right)  $z/\lambda = 0, 53, 105, 158$ ; solid and dashed lines are HG profile and numerical solutions, respectively. (c, f) Relative error between the profiles in (b, e). Top and bottom graphs are computed for  $w_0/\lambda = 0.5$  and  $w_0/\lambda = 2$ , respectively. Here  $\epsilon_{||} = 2.89$ ,  $\epsilon_{\perp} = 2.25$ . Inset: unit vectors  $s$  and  $t$ .

Fig. 2 (a) Computed transverse profile of  $\text{Re}(\mathbf{S})$  along  $s$  and (b) relative error with respect to the paraxial expression for  $w/\lambda = 0.5$ ;  $\text{Re}(\mathbf{S})$  is normalized to its peak for fixed  $z$  and each curve corresponds to the same  $z/\lambda$  of Fig. 1. (c) Ratio of maxima of  $|E_t|$  and  $|E_s|$  for fixed  $z$  and (d) ratio between maxima of odd and even parts of  $\text{Re}(\mathbf{S})$  vs  $w_0/\lambda$ .

Fig. 3 Soliton self-steering in NLC. (a) Soliton waist (dashed blue line) and walk-off (solid green line) versus power density. (b) Plots of  $|H_x|$  and the optical perturbation  $Dq$  in the soliton case, versus  $y$  and the logarithm of the power density  $P_d$ , with  $P_d=62$  W/m. Both quantities are normalized to their peak value at each power. (d) Beam evolution in  $yz$  computed by BPM when the input profile corresponds to a solitary solution for  $P_d = 62$  W/m (black lines, beam with the largest slope in  $yz$ ) and  $P_d = 1.8 \cdot 10^4$  W/m (red lines). (c) and (d) show the corresponding perturbation in the director distribution in the cell.

### List of Symbols, Abbreviations and Acronyms

NL: nonlinear

NLC: nematic liquid crystals

E7: commercial mixture of nematic liquid crystals (supplied by Merck)

SVEA: slowly varying envelope approximation

(1+1)D: one (transverse) plus one (propagation) dimensions in space

BPM : beam propagation method

### Appendix: confirmation of expenditures

I confirm that expenditures in excess of US\$20,000.00 were incurred for during the first months of the Project started last September 1, 2010, including overhead, consumables, equipment, travel and personnel.

Sincerely,

Prof. Gaetano Assanto



**Grant # FA8655-10-1-3010**

**NATO-EAORD Project**

**“Re-addressable Interconnects with Light-induced Waveguides in Liquid Crystals”**

## **Second Periodic Report**

**Prof. Gaetano Assanto**

**Nonlinear Optics and OptoElectronics Lab**

Department of Electronic Engineering, University Roma Tre  
Via della Vasca Navale 84, 00146 Rome- ITALY

### **Table of Contents**

Summary

1. Introduction

2. Methods, Assumptions, and Procedures

Self-Localized light propagation and Self-Steering via power dependent walkoff in nematic liquid crystals: model

3. Results and Discussion

Soliton Self-Steering via power dependent walkoff in nematic liquid crystals: experiments

4. Conclusions

5. References

6. List of Figures

List of Symbols, Abbreviations and Acronyms

Appendix: confirmation of expenditures

### **Summary**

In the second period of four months of the Project, various aspects of light self-localization in undoped nematic liquid crystals have been examined, with particular emphasis on the propagation of spatial solitons and their power-dependent self-steering via nonlinear changes in birefringent walkoff. For the experimental demonstrations of the results discussed hereby we employed samples prepared at the University of Southampton (UK) and at the Institut Non Lineaire de Nice (Sophia Antipolis, France)

After a brief introduction, we summarize the pillars of self-localized beam propagation in nematic liquid crystals, and then report on theory, numerical predictions and experimental results on transverse self-acceleration of spatial optical solitons in these uniaxial media.

### **1 Introduction**

Temporal and spatial self-localization of light are relevant topics in modern optics, for their implications in fundamental physics as well as their potential role in new generations of communication-oriented all-optical technologies.

In the spatial domain, nonlinear confinement of light occurs when beam spreading due to diffraction is balanced by nonlinear self-focusing, giving rise to transversely finite beams preserving their profile in propagation, i.e. optical spatial solitons.[1] Shape and stability of a soliton depend on the specific kind of nonlinearity, and several physical mechanisms can sustain light self-trapping, including reorientation [2-3].

Dielectrics with a nonlocal response are of interest in light self-confinement primarily for the stabilizing effects on (2+1)D solitons, otherwise unstable in pure Kerr media. Nonlocality, often (but not exclusively) quantified by the ratio between the widths of the nonlinear perturbation and of the light-beam profile, can range from unity (local media) to nearly infinity (highly nonlocal media). In the latter limit, solitons or *Nematicons* have been observed in nematic liquid crystals (NLC) [2]. Nonlocality is also responsible for self-deflection of individual solitons via interactions with boundaries, as demonstrated by us in NLC. [4]

We report hereby on the investigation, both theoretical and experimental, of nematicon self-steering via nonlinear walk-off and its dependence on the initial orientation of the optic axis. In Sec. 2 we model self-confinement and self-steering of nematicons in the absence of losses, solving the nonlinear eigenvalue problem for various initial permittivity tensors (i.e. various orientations of the optic axis). In Sec. 3 we report our experimental results and compare them with numerical simulations accounting for losses.

## 2 Methods, Assumptions, and Procedures

### Self-Localized light propagation and Self-Steering via power dependent walkoff in nematic liquid crystals: model

Liquid crystals are mesophase dielectrics sharing properties of solids and liquids. The nematic liquid crystalline phase possesses the lowest symmetry, with a high degree of order in the angular orientation of the molecules but without positional order. We deal with uniaxial nematic liquid crystals, i.e., with one symmetry axis or *director*  $\mathbf{n}$ , refractive indices  $n_e$  and  $n_o$  along and normal to  $\mathbf{n}$ , respectively, with  $n_e < n_o$ . We assume  $\mathbf{n}$  to lie in the plane  $yz$ : thus, the angle  $\theta$  completely describes the distribution of the director. It is convenient to work with the magnetic field  $H$ , with only one non-zero component along  $\mathbf{n}$ , rather than the electric field  $E$ . Accounting for the high nonlocality of NLC stemming from intermolecular links in the liquid crystal state, nonlinear optical propagation in the paraxial approximation is governed by

$$2ikn_e \partial A / \partial z + \tan \delta \partial A / \partial y + D_y \partial^2 A / \partial y^2 + \partial^2 A / \partial x^2 + k^2 \Delta n^2 A = 0, \quad (1)$$

$$\nabla^2 \theta + \gamma |E_t|^2 \sin[2(\theta - \delta)] = 0 \quad (2)$$

where  $k$  is the vacuum wavevector,  $\delta$  is the walkoff angle,  $n_e(\theta)$  is the extraordinary refractive index,  $D_y$  is the diffraction coefficient,  $A$  is the slowly varying envelope,  $\Delta n^2$  accounts for the light-induced index well,  $E_t$  is the electric field component orthogonal to the Poynting vector, and  $\gamma = \epsilon_0(n_o^2 - n_e^2)/(4K)$ , with  $K$  the Frank elastic constant for molecular deformations. Eq. (2) governs the director reorientation  $\theta$ ;  $\theta$  affects the electromagnetic propagation by modifying the (extraordinary) refractive index Eq. (1). At variance with purely Kerr media, the relationship between refractive index changes and intensity, stemming from Eq. (2), is nonlinear. Specifically, from the sine term we expect a saturable behavior versus power, strongly dependent on the initial conditions. For  $\Phi$  the optical perturbation, we can therefore set  $\theta = \theta_0 + \Phi$ , with  $\theta_0$  a constant; determined by the molecular anchoring via chemi-mechanical treatments of the interfaces bounding the NLC layer.

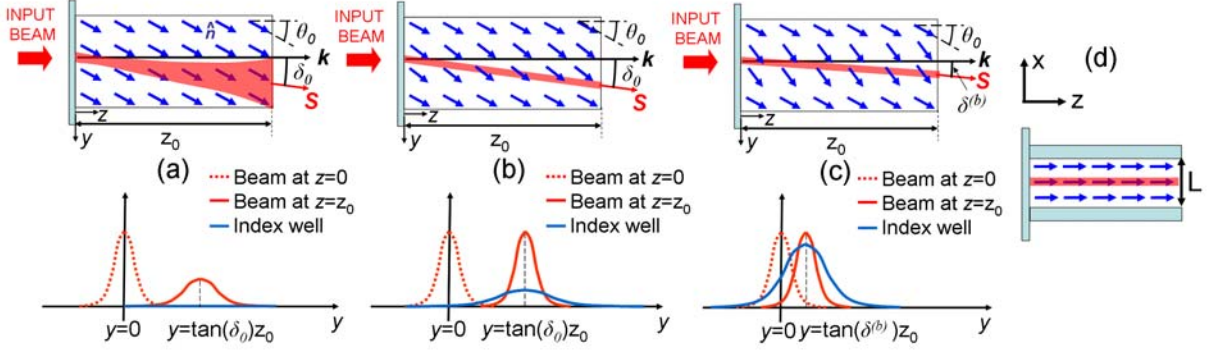


Fig. 1. (a) Beam diffraction in the linear regime. (b) Soliton formation without changes in walk-off. (c) Soliton self-steering with (high) input power. (d) Side view of a typical planar cell.

We can identify three different regimes for light propagation. At very low powers,  $\Phi$  is small, thus in the linear regime the beam diffracts and has a Poynting vector at an angle  $\delta$  with respect to  $z$  [Fig. 1(a)]. When the power increases,  $\Phi$  grows self-confinement occurs, but is still small with respect to  $\theta_0$  and does not affect the walk-off [Fig. 1(b)]: this is the perturbative nonlinear regime. For further increases in power,  $\Phi$  becomes comparable with  $\theta_0$  and  $\delta$  depends on power, i. e. nematicon self-steering take place due to nonlinear variations in walk-off [Fig. 1(c)]: this regime is no longer perturbative.

The system of Eqs. (1-2) is a full 3D model, with no approximations. To simplify the treatment we reduce it to an effective 2D model by considering a standard planar cell of thickness  $L$  [Fig. 1(d)] and a nematicon propagating in the mid-plane  $x=L/2$ , where no forces are exerted by the boundaries. Using such an effective 2D model, looking for nematicon profiles versus  $\theta_0$  and excitation power, we consider a power-dependent walk-off, i.e. solitons in the form  $\Theta_u = u(y) \exp(ik_{NL}z)$ ,  $\Phi(x,y,z) = \phi(y,z) \sin(\pi x/L)$ ,  $\phi = \phi_u(y')$ , where  $y' = y - z \tan \delta$ . The resulting model yields

$$2n_{NL}n_e k^2 u = D_y \partial^2 u / \partial y'^2 + k^2 n^2_e u \quad (3)$$

$$(1 + \tan^2 \delta) \partial^2 \phi_u / \partial y'^2 - (\pi/L)^2 \phi_u + \gamma (Z_0 / (n_e \cos \delta) \sin(2(\phi_u + \theta_0 - \delta))) |u|^2 = 0 \quad (4)$$

In the perturbative regime  $u$ ,  $\phi$  and  $n_e$  suffice to fully characterize a nematicon, whereas in the nonperturbative regime  $\delta$  needs be found, as well.

Simplified solutions for the nematicon profiles can be found in the highly nonlocal limit, i.e. when a parabolic profile can be used for the nonlinear optical perturbation.

The system of Eqs. (3-4) was numerically solved with an iterative algorithm for nonlinear eigenvalue problems; at each cycle, the walkoff  $\delta$  was updated based on the last computed  $\phi_u$ , i.e. accounting for its nonlinear variations. Sample results for the lowest-order self-confined beam at a wavelength of 1064nm are shown in Figs. (2-3). The soliton  $|u|^2$  has a Gaussian shape, consistently with the hypothesis of high nonlocality, whereas the nonlinear index well  $\phi_u$  is proportional to  $\exp(-\pi|y'/L|)$ . Nematicon waist and walkoff versus  $\theta_0$  and power  $P$  are plotted in Fig. 3 and agree well with the theoretical predictions.

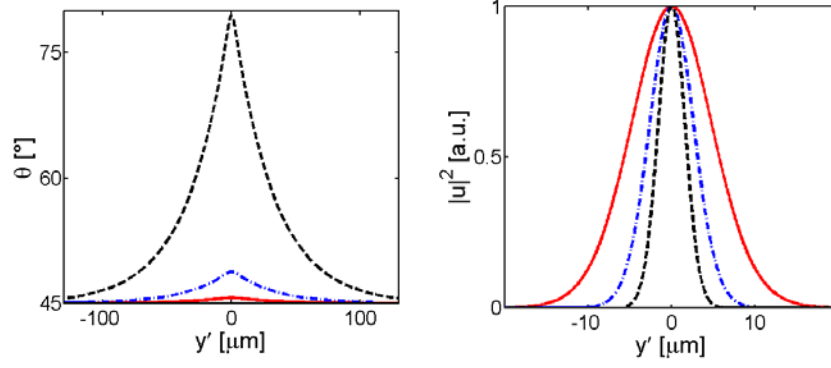


Fig. 2. Director distribution  $\theta_0 + \phi_u$  (left) and corresponding soliton profile  $|u|^2$  (right) versus  $y'$  for  $P=0.1$  (solid red line)  $0.5$  (dashed-dotted blue line) and  $10\text{mW}$  (dashed black line).

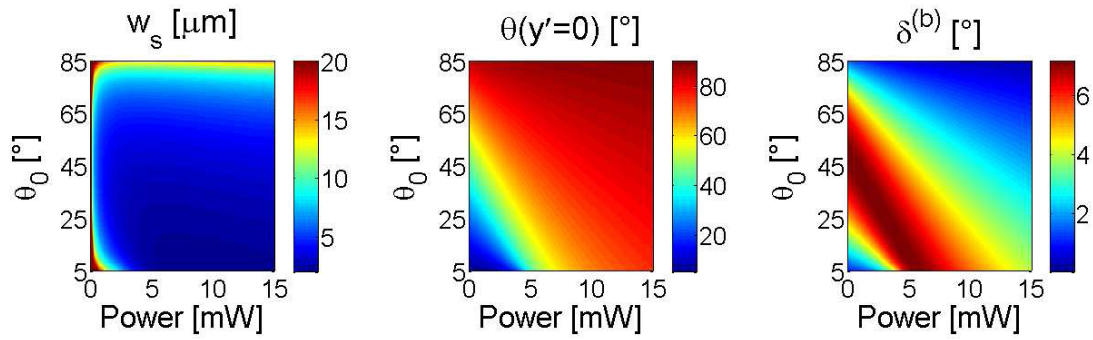


Fig. 3. From left to right: plots of soliton waist, maximum reorientation angle and walk-off versus  $P$  and  $\theta_0$ .

### 3. Results and Discussion

#### Soliton Self-Steering via power dependent walkoff in nematic liquid crystals: experiments.

As pointed out in the previous section, the model predicts soliton self-steering owing to nonlinear changes in walk-off. The latter phenomenon was recently addressed experimentally in Ref. 5 using a sample with an orientation  $\theta_0=80^\circ$  to optimize the observable beam deviation versus power: hereby we extend the study to various  $\theta_0$

In the experiments we used  $100\mu\text{m}$ -thick planar cells filled with the commercial E7, with birefringence  $\Delta n=0.2$ . Upper and lower glass interfaces parallel to the beam propagation plane  $yz$  were treated in order to achieve various orientations of the molecular director in the bulk NLC. We focused an infrared beam from a Nd:YAG laser operating at  $1064\text{nm}$  to a waist of about  $5\mu\text{m}$ , coupling it into the sample with wavevector parallel to  $z$  and in the midplane  $x=L/2$ ; using the out-of-plane scattered light, with a microscope objective lens and a CCD camera we studied the beam evolution in  $yz$  as a function of input power and initial orientation  $\theta_0$ . When varying the excitation and the orientation, we avoided powers high enough to induce transverse instabilities and/or excessive beam fluctuations, averaging our observations over a large number of acquisitions. Power dissipation in the samples due to scattering was the only significant departure of our data from the predictions illustrated in the previous section. To correctly interpret the results, the beam power  $P$  was expressed as  $P=P_0\exp(-2\alpha z)$ , with  $P_0$  the input excitation in  $z=0$  and  $\alpha$  the loss coefficient, evaluated to

about  $5 \text{ cm}^{-1}$  in our samples. Due to losses, in the nonperturbative regime the strong reorientation is gradually reduced and, thus, the nonlinear walkoff is non-uniform along  $z$ , giving rise to bent trajectories until, for large  $z$  and back in a perturbative regime, they become all parallel to the linear Poynting vector.

Figs. (4) and (5) show the beam evolution and acquired trajectories for various  $\theta_0$  and  $P_0$ . For  $\theta_0=80^\circ$ , even if the nonlinearity was low (self-confinement is weak) we observed large self-steering, because a small reorientation produces a large variation of walk-off: at low excitations the trajectory has no power dependence, while for  $P_0$  close to 20mW the walk-off changes owing to large reorientation. For  $\theta_0\approx 70^\circ$  the observed displacement is comparable with the previous one, although transverse instabilities limit the observation to powers below 30mW: the trade-off between nonlinearity and power-dependent walk-off results in the largest soliton steering.

For  $\theta_0\approx 45^\circ$  the nonlinearity increases towards its peak (the highest nonlinear index well for a fixed power in the perturbative regime), but variations in walkoff decrease: self-steering exhibits a relative minimum versus  $\theta_0$ , with excitation limited to 10mW by instabilities. Smaller  $\theta_0$  allow appreciable soliton steering. From Fig. (5) we also infer that walk-off variations versus power are positive for  $\theta_0>45^\circ$  and negative otherwise.

To model the role of losses on soliton propagation we used a beam propagator and an additional attenuation term depending on  $\alpha$ ; the nonlinear changes in permittivity were evaluated from the boundary problem with a relaxation algorithm; the two solvers ran iteratively until convergence was reached. The beam trajectories are plotted in Fig. (6), with an optimum agreement between theory and experiments obtained with a fit-coefficient larger than 1 on soliton power. A comparison between measured and predicted power-dependent variations in walk-off can be carried out by considering the self-steering in early stages of propagation and at different powers for all  $\theta_0$ , namely  $P_0=2, 5$  and 10mW.

#### 4 Conclusions

We have investigated soliton self-steering in undoped nematic liquid crystals with various initial orientations in the plane of propagation, i.e. self-deflection of nematicons owing to power-dependent reorientation of the optic axis. We introduced perturbative and non-perturbative regimes, the latter accounting for all-optical changes in walk-off. We reduced the complete 3D system to an equivalent 2D model retaining nonlocality. In the perturbative regime, we found two scalar parameters describing soliton waist and walk-off versus  $\theta_0$ .

To verify the predictions, we experimentally investigated nematicon propagation and self-steering in samples with various  $\theta_0$ , obtaining an excellent agreement between data and numerics even in the presence of scattering losses which induce a decay of the nonlinear response along propagation.

## 5 References

- <sup>1</sup> C. Conti and G. Assanto, in *Encyclopedia of Modern Optics*, Vol. 5, pp. 43-55, edited by R. D. Guenther, D. G. Steel and L. Bayvel, (Elsevier, Oxford, 2004)
- <sup>2</sup> G. Assanto and M. Karpierz, *Liq. Cryst.* **36**, 1161 (2009)
- <sup>3</sup> M. Peccianti, C. Conti, G. Assanto, A. De Luca and C. Umeton, *Appl. Phys. Lett.* **81**, 3335 (2002)
- <sup>4</sup> A. Alberucci, M. Peccianti, and G. Assanto, *Opt. Lett.* **32**, 2795 (2007).
- <sup>5</sup> A. Piccardi, A. Alberucci, and G. Assanto, *Appl. Phys. Lett.* **96**, 061105 (2010).

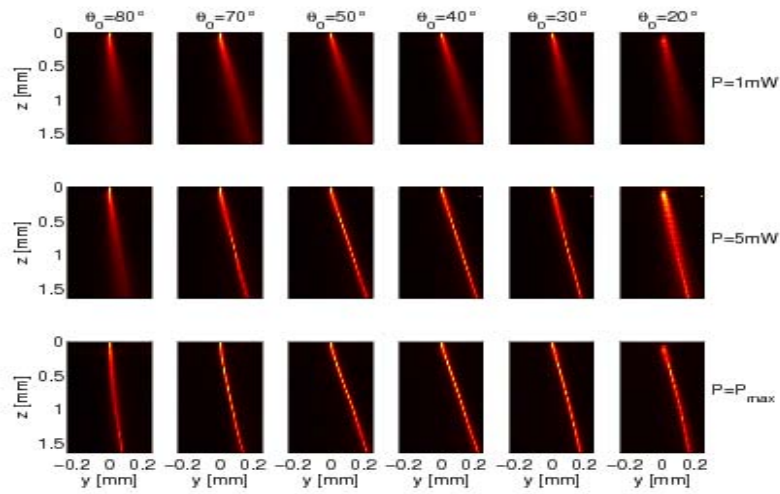


Fig. 4. Photographs of beam evolution for several initial angles  $\theta_0$  and power.  $P_{\text{MAX}}$  indicates the maximum power before instabilities kicked-in.  $P_{\text{MAX}} = [60 \ 30 \ 10 \ 10 \ 10 \ 30]\text{mW}$  for  $\theta_0 = [80 \ 70 \ 50 \ 40 \ 30 \ 20]^\circ$ , respectively.

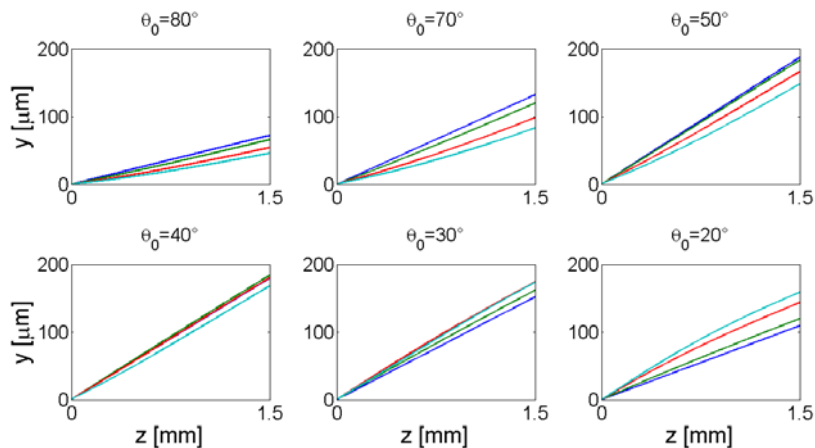


Fig. 5. Acquired beam trajectories and their dependence on  $\theta_0$  and  $P_0$ . Panels (a-f) correspond to  $\theta_0 = 80^\circ, 70^\circ, 50^\circ, 40^\circ, 30^\circ$  and  $20^\circ$ , respectively. Blue, green and red lines correspond to  $P = 1, 5, 10\text{mW}$ . The cyan line (where present) corresponds to the maximum usable excitation,  $P_0 = 60\text{mW}$  for  $\theta_0 = 80^\circ$  and  $P_0 = 30\text{mW}$  for  $\theta_0 = 70^\circ$  and  $20^\circ$ , respectively.

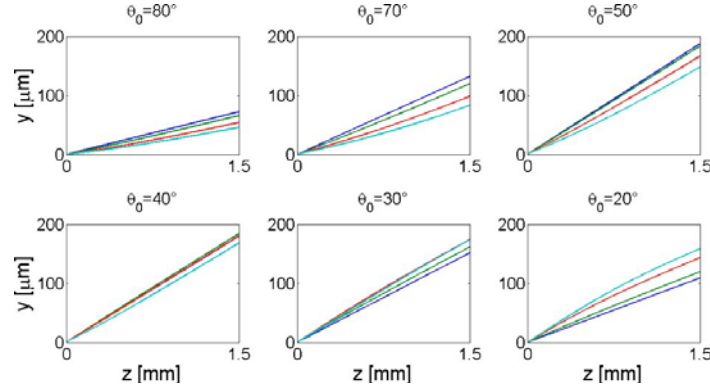


Fig. 6. Numerically computed soliton trajectory in the plane  $yz$  for various  $\theta_0$  and  $P_0 \rightarrow 0$  mW (blue line),  $P_0 = 1$  mW (green line),  $P_0 = 3$  mW (red line) and  $P_0 = 5$  mW (cyan line) versus  $\theta_0$ . The parameters are consistent with the experimental values.

## 6. List of figures

Fig. 1. (a) Beam diffraction in the linear regime. (b) Soliton formation without changes in walk-off. (c) Soliton self-steering with (high) input power. (d) Side view of a typical planar cell.

Fig. 2. Director distribution  $\theta_0 + \phi_u$  (left) and corresponding soliton profile  $|u|^2$  (right) versus  $y'$  for  $P=0.1$  (solid red line) 0.5 (dashed-dotted blue line) and 10 mW (dashed black line).

Fig. 3. From left to right: plots of soliton waist, maximum reorientation angle and walk-off versus  $P$  and  $\theta_0$ .

Fig. 4. Photographs of beam evolution for several initial angles  $\theta_0$  and power.  $P_{MAX}$  indicates the maximum power before instabilities kicked-in.  $P_{MAX} = [60 \ 30 \ 10 \ 10 \ 10 \ 30]$  mW for  $\theta_0 = [80 \ 70 \ 50 \ 40 \ 30 \ 20]^\circ$ , respectively.

Fig. 5. Acquired beam trajectories and their dependence on  $\theta_0$  and  $P_0$ . Panels (a-f) correspond to  $\theta_0 = 80^\circ, 70^\circ, 50^\circ, 40^\circ, 30^\circ$  and  $20^\circ$ , respectively. Blue, green and red lines correspond to  $P = 1, 5, 10$  mW. The cyan line (where present) corresponds to the maximum usable excitation,  $P_0 = 60$  mW for  $\theta_0 = 80^\circ$  and  $P_0 = 30$  mW for  $\theta_0 = 70^\circ$  and  $20^\circ$ , respectively.

Fig. 6. Numerically computed soliton trajectory in the plane  $yz$  for various  $\theta_0$  and  $P_0 \rightarrow 0$  mW (blue line),  $P_0 = 1$  mW (green line),  $P_0 = 3$  mW (red line) and  $P_0 = 5$  mW (cyan line) versus  $\theta_0$ . The parameters are consistent with the experimental values.

## List of Symbols, Abbreviations and Acronyms

NL: nonlinear

NLC: nematic liquid crystals

E7: commercial mixture of nematic liquid crystals (supplied by Merck)

SVEA: slowly varying envelope approximation

(1+1)D: one (transverse) plus one (propagation) dimensions in space

BPM: beam propagation method

**Appendix: confirmation of expenditures**

I confirm that expenditures in excess of US\$20,000.00 were incurred for during the second four months (January-April 2011) of the Project started last September 1, 2010, including overhead, consumables, equipment, travel and personnel.

Sincerely,

Prof. Gaetano Assanto

A handwritten signature in black ink, appearing to read "Gaetano Assanto". The signature is fluid and cursive, with the first name "Gaetano" written in a larger, more prominent script than the last name "Assanto".

**Grant # FA8655-10-1-3010**

**NATO-EAORD Project**

**“Re-addressable Interconnects with Light-induced Waveguides in Liquid Crystals”**

## **Third and Final Periodic Report**

**Prof. Gaetano Assanto**

**Nonlinear Optics and OptoElectronics Lab**

Department of Electronic Engineering, University Roma Tre  
Via della Vasca Navale 84, 00146 Rome- ITALY

### **Table of Contents**

Summary

1. Introduction

2. Methods, Assumptions, and Procedures

Self-Localized beam propagation, refraction and total internal reflection at a voltage defined interface between two regions of nematic liquid crystals

3. Results and Discussion

Soliton waveguide electro-optic steering device: design and numerical experiments in standard E7

4. Conclusions

5. List of publications based on the Project

6. References

7. List of Figures

List of Symbols, Abbreviations and Acronyms

Appendix: confirmation of expenditures

Disclosure of inventions

### **Summary**

In the third four-month period of the Project, various aspects of transverse acceleration of self-confined light beams in undoped nematic liquid crystals have been examined, with particular emphasis on the maximization of power-dependent soliton self-steering through a dielectric interface defined by applied voltage in a planar liquid crystalline cell. After the modelling and the detailed numerical simulation of the problem, we designed a specific set of electrodes to maximize soliton waveguide deflection with electro-optic control. We expect angular deflections as large as 70 degrees at a single graded interface using the standard mixture E7.

After a brief introduction, we describe the model, the geometry and its advantages; we then report on the numerical results and expected performance on soliton steering upon refraction and total internal reflection.

## 1 Introduction

Owing to their unique properties intermediate between those of liquids and of solids, liquid crystals (LC) are relevant materials in optical signal processing; one of their remarkable features is their sensitivity to applied perturbations, such as electric fields. The latter provides large electro-optic and all-optical responses and significant tunability through molecular reorientation. Self-focusing in nematic LC (NLC), i.e. LC with a high degree of orientational order but no positional order has allowed generating reorientational spatial solitons or nematicons, i.e., non-diffracting self-confined beams, at mW powers.[1] Nematicons are light-induced waveguides with nonlocal features providing stability, robustness and long range interactions, even with partially incoherent light. Such light-induced channels can confine and route weaker copolarized signals of arbitrary wavelengths and transmission protocols; they can form a reconfigurable fabric of interconnections in circuits defined by light and with paths controlled by light and/or by voltage(s).

We analyze a scheme for the effective angular deflection of self-guided beams, using NLC and voltage-driven dielectric interfaces to obtain the steering of spatial soliton waveguides over angles as large as  $70^\circ$ . We resort to a double set of comb-patterned electrodes to achieve in-plane nematicon propagation and steering, by bias-tuning the effective anisotropy and avoiding the detrimental effects of out-of-plane walk-off.

Electro-optic beam deflectors with large angles were previously demonstrated in LC, [2,3]; however, the use of nematicons with waist of a few  $\mu\text{m}$  permits the deflection of guided-wave signals irrespective of their spectral placement and temporal format while maximizing the number of resolvable output spots.

## 2 Methods, Assumptions, and Procedures

### **Self-Localized beam propagation, refraction and total internal reflection at a voltage defined interface between two regions of nematic liquid crystals**

The planar geometry is sketched in Fig. 1: a nematic liquid crystal layer is confined between two glass slides parallel to plane  $yz$ , separated by  $L$  along  $x$  and treated at the glass/NLC interfaces to ensure the uniform orientation of the optic axis  $\mathbf{n}$  (i.e. the molecular director at an angle  $\theta_0$  with  $z$ ). At each interface, two interdigitated sets of electrodes with fingers along  $y$  and period  $\Lambda$  permit the application of low frequency electric fields. Each electrode pair on a given interface has a ground terminal in  $y=0$ , such that a voltage  $V_1$  ( $V_2$ ) on the left (right) comb can electro-optically twist the NLC molecular dipoles and therefore reorientate the optic axis in the plane  $yz$  and throughout the layer thickness in the region underneath.

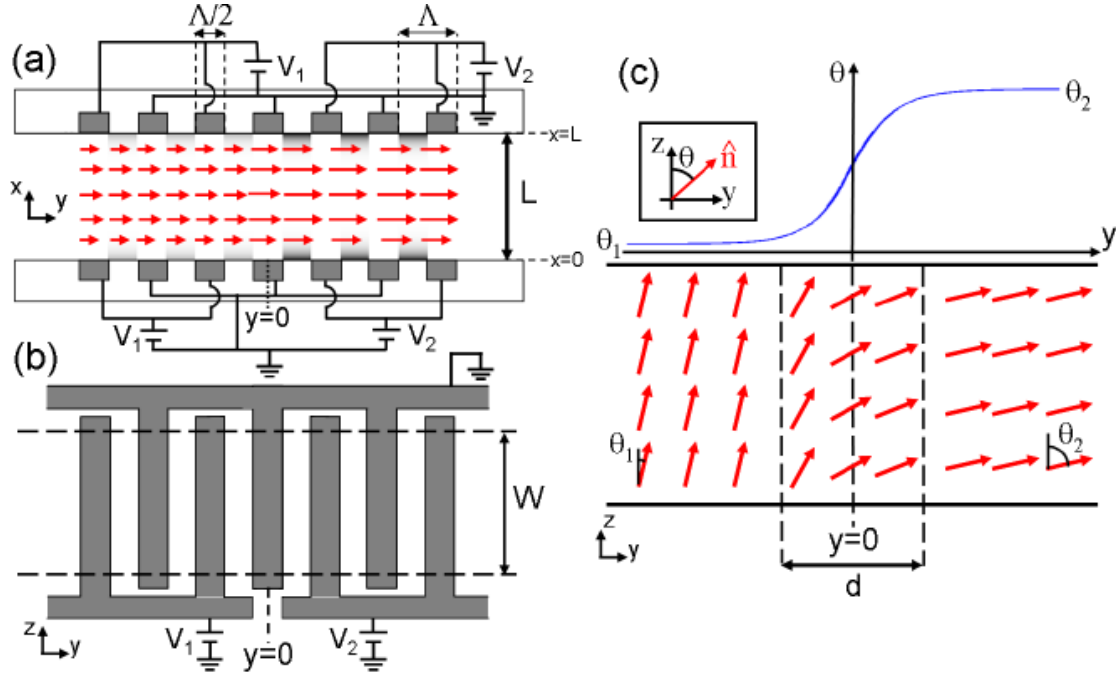


Figure 1. Sketch of the device. (a) Front view; the superposed grey-scale map represents the intensity of  $E_{LF}$  (black is the highest). (b) Top view of the electrodes. (c) Distribution of the NLC optic axis in the cell mid-plane  $x=L/2$  (bottom) and corresponding  $\theta$  versus  $y$  (top). Inset: definition of  $\theta$ . The red arrows indicate the orientation of the molecular director.

For  $\Lambda \ll L$ , the dominant component of the applied electric field is along  $y$ , thus  $\mathbf{n}$  tends to rotate in the plane  $yz$  and align with the field polarization. To first approximation, at each NLC/glass interface  $E_{LF}(x=0)=E_{LF}(x=L)=0$  under the electrodes and  $E_{LF}(x=0)=E_{LF}(x=L)=2V_{1,2}/\Lambda$  in between them; the  $E_{LF}$  distribution for  $V_2 > V_1$  is represented in Fig. 1(a). Owing to the NLC electro-optic response to  $E_{LF}$  the optic axis  $\mathbf{n}$  will be twisted everywhere in the same way. Moreover, the nonlocal character of the elastic response, in the limit  $\Lambda \ll L$ , will smooth out the spatial inhomogeneities of  $E_{LF}$ , making the bias-driven reorientation voltage-tuned in the two regions across  $y=0$  and uniform through the cell thickness. Therefore, applied biases  $V_{1,2}$  give rise to a graded interface along  $y$  [see Fig. 1(c)], of width  $d$  depending on  $L$  and with an electrically controlled change in director angle.

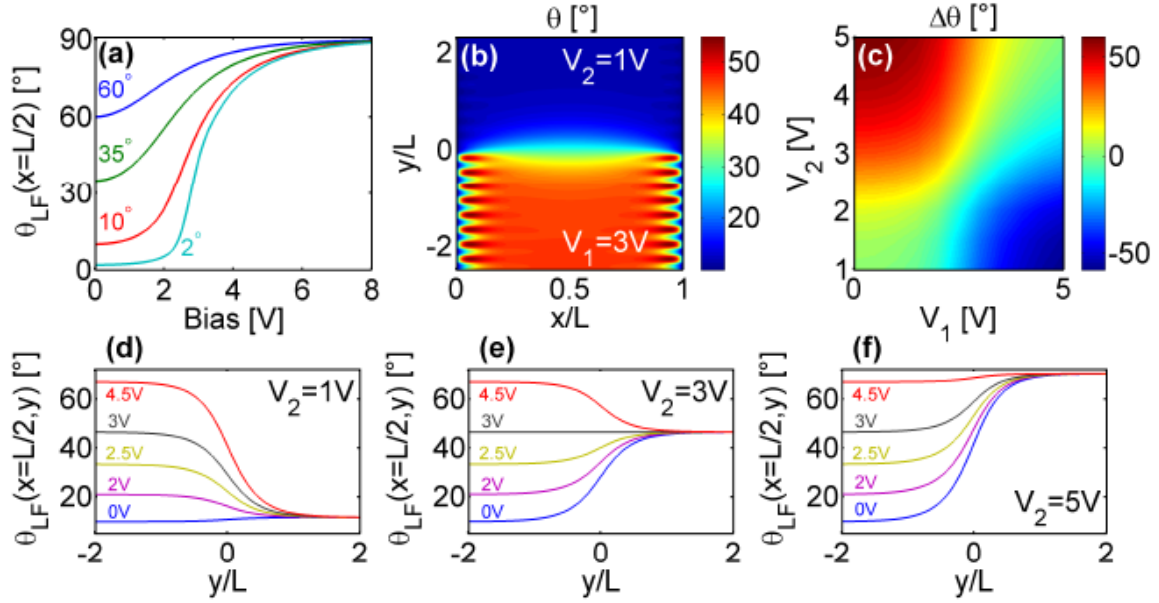


Figure 2. (a) Reorientation angle in the cell mid-plane  $x=L/2$  for  $V_1=V_2$  versus applied bias: each label indicates the corresponding background angle  $\theta_0$ ; (b) color map of  $\theta$  in the plane  $xy$  and (c) maximum change in  $\theta$  ( $x=L/2, y$ ) versus applied biases  $V_1$  and  $V_2$ . (d-f):  $\theta$  distribution versus  $y$  in  $x=L/2$  for various  $V_2$ . The labels on each line indicate the corresponding  $V_1$ . The bias values refer to a thickness  $L=100\mu\text{m}$ .

We numerically solved the NLC reorientational equation

$$\frac{\partial^2 \theta_{LF}}{\partial x^2} + \frac{\partial^2 \theta_{LF}}{\partial y^2} + \gamma_{LF} \sin(2\theta_{LF}) |E_{LF}|^2 = 0,$$

with  $\theta_{LF}$  the electro-optic reorientation,  $\gamma_{LF} = \Delta\epsilon_{LF}/[2K]$  with  $\Delta\epsilon_{LF}$  the low-frequency dielectric anisotropy and  $K$  the elastic constant. We chose the parameters of the commercial NLC mixture E7, with  $\gamma_{LF} = 5.4V^{-2}$ ; we also employed  $\sigma = 3.3$ . To trade off voltage-sensitivity (the Coulombian torque is maximum for  $\theta_0 = 45^\circ$ ) and the  $\theta$  variation across the interface, we set  $\theta_0 = 10^\circ$  [see reorientation curves in Fig. 2a]. As expected,  $\theta$  is constant near the mid-plane  $x=L/2$  and undergoes a negative (positive) variation  $\Delta\theta$  along  $y$  for  $V_1 > V_2$  ( $V_1 < V_2$ ) [Fig. 2c], with a quasi-linear trend over a transition length  $d \sim L$ , independent on bias.

Having established the link between voltages and  $\theta$  distribution, i.e. refractive index for extraordinarily polarized light, we turn to nonlinear propagation of beams launched in  $y < 0$  (where the index gradient is negligible) with wave vector  $\mathbf{k}$  at an angle  $\alpha$  with  $z$  in the plane  $x=L/2$  and extraordinary field polarized along  $y$ . Such excitation can reorientate the optic axis in the plane  $yz$ , i.e. ensuring in-plane director rotations and corresponding in-plane changes of walk-off. We stress that the spatial soliton trajectory after the interface does not depend on the profile of the transition region but simply on  $\Delta\theta$ , the specific distribution of  $\theta_{LF}$  only affecting the lateral displacement of the beam.

Nonlinear reorientation in  $yz$  and self-confined nematicon dynamics can be modelled in 2D by

$$2ik_0n_0 \left( \frac{\partial A}{\partial z} + \tan \delta \frac{\partial A}{\partial y} \right) + D_y \frac{\partial^2 A}{\partial y^2} + k_0^2 \Delta n_e^2 A = 0$$

$$\frac{\partial^2 \psi}{\partial z^2} + \frac{\partial^2 \psi}{\partial y^2} - \left( \frac{\pi}{L} \right)^2 \psi + \gamma \sin [2(\theta_{LF} + \psi - \delta)] |A|^2 = 0$$

with A the magnetic field along x,

$$\gamma = [\epsilon_0 / (4K)] (n_{\parallel}^2 - n_{\perp}^2) [Z_0 / (n_0 \cos \delta)]^2 \quad (Z_0 \text{ is the vacuum impedance}),$$

$\psi$  the (nonlinear) perturbation on  $\theta$  due to light (i.e.,  $\theta = \theta_{LF} + \psi$ ),

$D_y$  the diffraction coefficient,  $\delta$  the walk-off,  $k_0$  the vacuum wavenumber,  $n_0$  the extraordinary index and

$$\Delta n_e^2 = n_e^2(\theta) - n_0^2 \quad \text{the overall refractive index change.}$$

The nematicon trajectory can be calculated using the Ehrenfest's theorem.

### 3. Results and Discussion

#### Soliton waveguide electro-optic steering device: design and numerical experiments in standard E7

We assumed a linear profile for  $\theta_{LF}$  across d, from  $y=0$  to  $y=L=100 \mu\text{m}$ . Fig. 3a shows the evolution of a Gaussian beam launched in  $y=-50 \mu\text{m}$  with  $k//z$ . For  $\theta_1 > \theta_2$  the refractive gradient is negative, thus the soliton wave vector bends towards  $y < 0$ ; to achieve TIR, the change in  $k$  has to ensure a Poynting vector  $S$  leaving the interface with a negative  $y$  component. Noteworthy, reflection and incidence angles are generally different owing to anisotropy. For  $\theta_1 < \theta_2$ , conversely, the beam can always overcome the index barrier and be refracted.

Fig. 3b graphs the calculated soliton trajectories versus input power: the visible power dependence is due to all-optical changes in walk-off. For excitation with  $k//z$  the angle  $\beta$  of the Poynting vector with  $z$  away from the interface, the overall steering (from refraction to TIR) amounts to about  $40^\circ$  [Fig. 3c-d], with excellent agreement between the results from a beam propagator (BPM) and the predictions of the geometric optics approximation (GOA) for  $\beta$  up to  $20^\circ$ . Even larger deflections are obtained by launching solitons with phase fronts slanted with respect to  $z$ , i.e. nonzero  $\alpha$ .

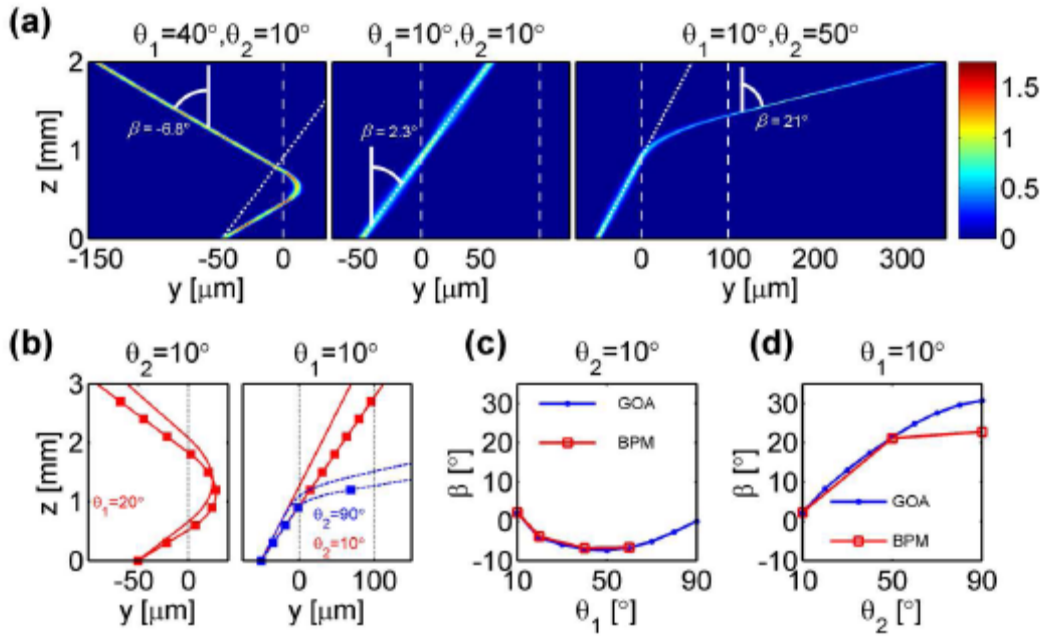


Figure 3. (a) Nematicon evolution for  $P=3\text{mW}$ ; dashed and dotted white lines indicate the interface borders and the beam trajectory when  $\theta_{LF}=10^\circ$ , respectively. (b) Left: trajectories upon TIR for  $P=0.5\text{mW}$  (no symbols) and  $P=3\text{mW}$  (squares); right: dashed (solid) lines correspond to  $\theta_2=90^\circ$  ( $10^\circ$ ). Soliton output slope  $\beta$  versus  $\theta_1$  for  $\theta_2=10^\circ$  (c) and versus  $\theta_2$  for  $\theta_1=10^\circ$  (d). The wavelength is  $1064\text{nm}$ , the input waist  $5\mu\text{m}$  and  $L=100\mu\text{m}$ .

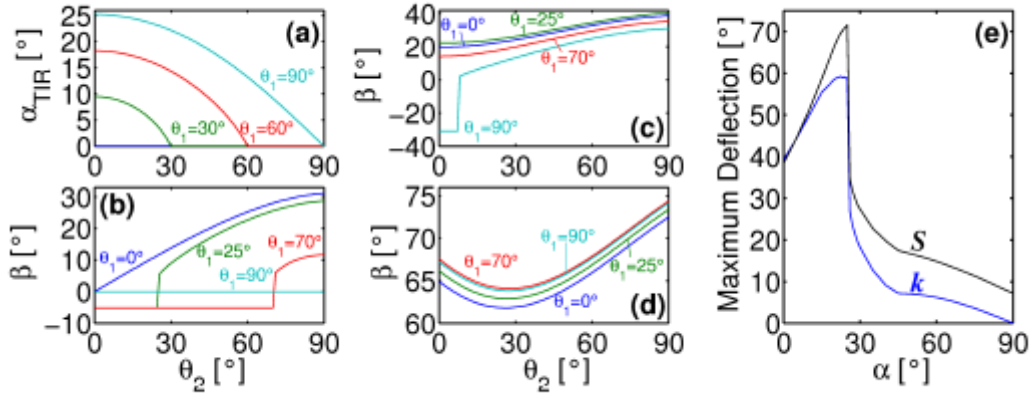


Figure 4. (a) TIR region vs  $\theta_1$  and  $\theta_2$ . Angle  $\beta$  versus  $\theta_2$  for  $\alpha=0$  (b),  $25^\circ$  (c) and  $70^\circ$  (d); the labels indicate the corresponding  $\theta_1$ . (e) Maximum angular deflection of wave vector and Poynting vector versus  $\alpha$ .

For a fixed  $\alpha$ , the crucial requisite to achieve large steering is the occurrence of TIR. Defining  $\alpha_{TIR}$  the maximum angle of incidence resulting in TIR,  $\alpha_{TIR}$  is plotted in Fig. 4a for given  $\theta_{1,2}$ , with a maximum  $\alpha_{TIR}$  approximately equal to  $25.1^\circ$ ; above such curves TIR does not take place. The output angle  $\beta$  versus  $\theta_2$  and  $\theta_1$  is graphed in Fig. 4b-d: the largest deflections are obtained for  $\alpha < \max(\alpha_{TIR})$  [for a fixed  $\theta_1$  the solitons evolve from TIR to

refraction as  $\theta_2$  varies, see Fig. 4(b-c) rather than for  $\alpha > \max(\alpha_{\text{TIR}})$  [where only refraction occurs, see Fig. 4d], with a maximum steering of  $60^\circ$  for  $\alpha = \max(\alpha_{\text{TIR}})$  and  $\theta_1 = 90^\circ$ . By varying  $\theta_1$  as well, an overall steering angle of  $70^\circ$  is achieved for  $\max(\alpha_{\text{TIR}})$  [Fig. 4e], taking advantage of the dependence of the refraction angle from walk-off.

Such voltage-controlled angular deviations, to be achieved with biases of a few Volt, are among the largest observed at a single dielectric interface and well above the record value of  $40^\circ$  reported for spatial solitons.[4] Larger steering could be engineered by adopting more complex or multiple interfaces.

## 4 Conclusions

We introduce a novel concept for optical signal steering using spatial solitons and a voltage-tunable interface in nematic liquid crystals. The design ensures in-plane self-confined and signal guiding propagation and deflection over angles as large as  $70^\circ$  by employing modest voltages, enabling the realization of readdressable interconnections and spatial demultiplexers with a wide angular span while guaranteeing the transparent transmission of one or several signals with arbitrary wavelengths and modulations.

## 5 List of Publications based on the Project in International (ISI) Journals

- A. Alberucci and G. Assanto: “Nematicons beyond the perturbative regime“, *Opt. Lett.* 35 (15), 2520–2522 (2010)
- A. Piccardi, A. Alberucci and G. Assanto: “Power-dependent nematicon steering via walk-off“, *J. Opt. Soc. Am. B* 27 (11), 2398-2404 (2010)
- A. Alberucci and G. Assanto: “Non Paraxial Solitary waves in anisotropic dielectrics“, *Phys. Rev. A* 83, 033822 (2011)
- A. Alberucci and G. Assanto: “On Beam Propagation in Anisotropic Media: one-dimensional analysis“, *Opt. Lett.* 36 (3), 334-336 (2011)
- A. Alberucci and G. Assanto: “Non-paraxial (1+1)D spatial solitons in uniaxial media“, *Opt. Lett.* 36 (2), 193-195 (2011)
- A. Piccardi, A. Alberucci, N. Tabiryan and G. Assanto: “Dark Nematicons“, *Opt. Lett.* 36 (8), 1456-1458 (2011)
- W.-P. Zhong, M. Belić, G. Assanto, B. A. Malomed, and T. Huang: “Self-trapping of scalar and vector dipole solitons in Kerr media“, *Phys. Rev. A* 83, 043833 (2011)
- C. P. Jisha, A. Alberucci, R.-K. Lee, and G. Assanto: “Wave-Particle Duality of Optical Solitons interacting with defects“, *Opt. Lett.* 36 (10), 1848-1850 (2011)
- M. Kwasny, A. Piccardi, A. Alberucci, M. Peccianti, M. Kaczmarek, M. Karpierz and G. Assanto “Nematicon-nematicon interactions in a medium with tunable nonlinearity and fixed nonlocality“, *Opt. Lett.* 36 (13), 2566-2568 (2011)
- R. Barboza, A. Alberucci and G. Assanto: “Large electro-optic beam steering with Nematicons“, *Opt. Lett.* 36 (14), 2611–2613 (2011)
- G. Assanto, A. Alberucci and A. Piccardi: “Transverse self-acceleration of Nematicons: can a self-confined beam change its own path?”, *J. Nonl. Opt. Phys. Mat.*, submitted (in press)

## 6 References

- <sup>1</sup> G. Assanto and M. Karpierz, *Liq. Cryst.* **36**, 1161 (2009)
- <sup>2</sup> S. Khan and N. Riza, *Opt. Express* **12**, 868 (2004)
- <sup>3</sup> S. Davis, G. Farca, S. Rommel, A. Martin, and M. Anderson, *Proc. SPIE* **6971**, 69710G (2008).
- <sup>4</sup> M. Peccianti, A. Dyadyusha, M. Kaczmarek, and G. Assanto, *Nat. Phys.* **2**, 737 (2006).

## 7. List of figures

Figure 1. Sketch of the device. (a) Front view; the superposed grey-scale map represents the intensity of  $E_{LF}$  (black is the highest). (b) Top view of the electrodes. (c) Distribution of the NLC optic axis in the cell mid-plane  $x=L/2$  (bottom) and corresponding  $\theta$  versus  $y$  (top). Inset: definition of  $\theta$ . The red arrows indicate the orientation of the molecular director.

Figure 2. (a) Reorientation angle in the cell mid-plane  $x=L/2$  for  $V_1=V_2$  versus applied bias: each label indicates the corresponding background angle  $\theta_0$ ; (b) color map of  $\theta$  in the plane  $xy$  and (c) maximum change in  $\theta$  ( $x=L/2, y$ ) versus applied biases  $V_1$  and  $V_2$ . (d-f):  $\theta$  distribution versus  $y$  in  $x=L/2$  for various  $V_2$ . The labels on each line indicate the corresponding  $V_1$ . The bias values refer to a thickness  $L=100\mu\text{m}$ .

Figure 3. (a) Nematicon evolution for  $P=3\text{mW}$ ; dashed and dotted white lines indicate the interface borders and the beam trajectory when  $\theta_{LF}=10^\circ$ , respectively. (b) Left: trajectories upon TIR for  $P=0.5\text{mW}$  (no symbols) and  $P=3\text{mW}$  (squares); right: dashed (solid) lines correspond to  $\theta_2=90^\circ$  ( $10^\circ$ ). Soliton output slope  $\beta$  versus  $\theta_1$  for  $\theta_2=10^\circ$  (c) and versus  $\theta_2$  for  $\theta_1=10^\circ$  (d). The wavelength is  $1064\text{nm}$ , the input waist  $5\mu\text{m}$  and  $L=100\mu\text{m}$ .

Figure 4. (a) TIR region vs  $\theta_1$  and  $\theta_2$ . Angle  $\beta$  versus  $\theta_2$  for  $\alpha=0$  (b),  $25^\circ$  (c) and  $70^\circ$  (d); the labels indicate the corresponding  $\theta_1$ . (e) Maximum angular deflection of wave vector and Poynting vector versus  $\alpha$ .

## List of Symbols, Abbreviations and Acronyms

NL: nonlinear  
LC: liquid crystals  
NLC: nematic liquid crystals  
E7: commercial mixture of nematic liquid crystals (supplied by Merck)  
BPM: beam propagation method  
GOA: Geometric optics approximation

## Appendix: confirmation of expenditures

I confirm that expenditures in excess of US\$20,000.00 were incurred for during the third four-month period (May-August 2011) of the Project started last September 1, 2010, including overhead, consumables, equipment, travel and personnel.

## Disclosure of inventions

I certify that there were no subject inventions to declare during the performance of this grant.

Sincerely,

Prof. Gaetano Assanto

